ISSN 1 746-7233, England, UK
World Journal of Modelling and Simulation
Vol. 10 (2014) No. 4, pp. 293-307

CFD simulation for the feasibility study of a modified solar chimney applied for building space heating*

Shiv Lal †

Centre for Energy Studies, Indian Institute of Technology, Delhi 110016, India

(*Received October 10 2013, Accepted June 29 2014*)

Abstract. The building integrated Modified Solar Chimney (MSC) have been studied for building space heating. The Computational Fluid Dynamics (CFD) software (ANSYS WORBENCH 14.0) has been used for simulation and results are validated through experimental data, and mesh adoption is used for new chimney design approvals. From the CFD simulation, it is found that the lowest $(20-35°C)$ air temperature is at the middle of solar chimney gap and highest near the absorber plate $(45-65°C)$. The experimental room can be maintained between $10°C$ to $20°C$ in peak winter season, where ambient temperature was observed as $3°C$ to $8°C$. This modified solar chimney works as an air heater and it is a feasible option for space heating of building.

Keywords: solar chimney, stack effect, CFD etc.

1 Introduction

A Trombe wall is a system for indirect solar heat gain and it is good example of passive heating system for buildings. It consists of black colored wall of high thermal mass facing the sun, with glazing spaced in front to leave a small air space. The glazing traps the solar radiation like a greenhouse. Trombe wall are ideal for spaces where silence and privacy are desirable. Operating costs are non-existent, and maintenance costs should be very low. A successful Trombe wall or attached sunspace optimizes heat gain and minimizes heat loss during cold times, and avoids excessive heat gain in summer times.

The Trombe wall can be used as solar chimney for building ventilation. It can be modified for improving its performance and applications. Lal et al.[22] proposed some modification with providing air flow control (damper) arrangement and integration approaches with other type of passive systems. There are two dampers are provided at top and upper room vent. In winter top damper of the chimney closed to restrict the air flow towards room, and in summer upper room vent closed and chimney top damper opened to air exit in to atmosphere. Many studies have been carried out by various researchers but still this concept is not commonly used in building design till date. Few numerical and simulation studies presented by the researchers, and there is more simulation and parametric studies are required.

Trombe wall a type of passive solar home heating system was developed as preliminary solar chimney by Trombe and Michel[3] at the C. N. R. S. laboratory in France. Bansal et al.[6] used it for building ventilation and developed a mathematical model to calculating air change per hour (ACH). Ong[26] developed heat transfer modelling of solar chimney for building ventilation and afterward Ong and Chow[27] presented the experimental study. Bouchair et al.[11] and Bouchair[10] explored the solar chimney to optimized the chimney width (one tenth of chimney height) for maximum air flow rate A simple solar chimney was studied for natural

* The author (Shiv Lal) gratefully acknowledges University College of Engineering, Rajasthan Technical University, Kota, Rajasthan (India) and IIT Delhi (India), for sponsorship under quality improvement program of government of India. Author also acknowledges Prof. S.C. Kaushik, CES, IIT Delhi and Dr. P.K. Bhargava, CBRI-Roorkee to supervise this research work.

† Corresponding author. *E-mail address*: shivlal1@gmail.com

ventilation of building with heat recovery using CFD techniques by Gan and Riffat[17]. In which ventilation rate, solar heat gain and glazing type were investigated for enhanced performance. It was observed that the double or triple glazed solar chimney gives higher ventilation effect than single glazed chimney. In continuation of that, a parametric study of Trombe wall for passive cooling of building was carried out by Gan[15]. The air gap was varied between $0.1m$ to $0.4m$ and the air flow rate equation proposed to calculating air flow rate, mass flow rate and effect of wall heat gain and heat storage height of chimney on air flow rate for particular condition.

Chen and Li[12] demonstrated the existence of an optimum air gap to height ratio and deliberated the result as that ratio depends on the chimney inlet design. It was stated that the large inlet size can be optimized as large air gap to height ratio. Khedari et al.[19] investigated the effect on ventilation (through solar chimney) of indoor fluctuation and air change in a school building in Thailand. The study was based on four solar chimney configurations namely: conventional Trombe wall; modified Trombe wall, Metallic solar wall (MSW) and roof solar collector. The study was conducted by using a $25m^3$ class room. The induced number of air change rate varied between $8 - 15$ and temperature was reduced by $2 - 3°C$ by MSW and modified arrangements. In the continuation of simulation studies, Barozi et al.[7] used a two dimensional computational fluid dynamics (CFD) method to investigate the air movement in a 1:12 building model and found a good agreement between simulation and experimental results. Awbi and Gan[4] used for turbulent flow model three dimensional simulation study of a solar chimney where a good agreement was achieved between simulated and Bouchair's[10] experimental air flow rates.

Zalewski et al. used TRANSYS library type 36 model for the study and validated by the experimental results[28]. The wall height and width was selected as $2.47m$ and $1.34m$ respectively, where massive wall thickness was 0.15m, massive wall conductivity selected for simulation as $0.8117W/m°C$ and all other parameters are clearly discussed in the same paper. The results shows that the composite wall has better energetic performance than the classical wall in cold/cloudy weather. Liping and Angui[24] used $k - \varepsilon$ model with standard functions for the test of reliability and accuracy of the turbulent model of $1.5m$ height and $0.62m$ air gap vertical solar chimney (width range varying between 0.1 to $0.62m$). The uniform solar flux was varied from $200W/m^2$ to $600W/m^2$. They proposed the optimum ratio of air gap to chimney height which is approximately 0.5, whereas the minimum chimney height proposed more than $1m$ for vertical collector.

Bacharoudis et al.[5] presented a study on natural convection phenomena inside a wall solar chimney with one wall adiabatic and one under a heat flux. Their main research focused on numerical study of buoyancy driven flow field inside the chimney and heat transfer analysis for turbulent flow model. The $k - \varepsilon$ model is likely to provide superior performance than other models for flow boundary layers under strong adverse pressure gradient that's why it was selected for simulation. Nouanegue et al.[25] re-counted the other performance affecting parameters as: Rayleigh number (Ra), Reynold number (Re) and the geometrical parameters like aspect ratio, the exit port size (h/L) and wall thickness. An analytical and numerical study of solar chimney used for improving natural ventilation was conducted by Bassiouny and Koura[9] in Egypt. Bassiouny et al.[8] developed a FORTRAN programme to optimize the chimney inclination angle and found between $45°$to $70°$ for latitude $28.4°$ for 0.1 to $0.35m$ chimney width and $500W/m^2$ solar intensity.

Zamora and Kaiser[29] numerical studied the natural convection in channels or solar chimney through CFD. They apply Reynolds $k - \omega$ turbulence model to simulate the turbulent case and the solar chimney was configured for vide range of Rayleigh number (varying between 10^5 to 10^{12} for symmetrical isothermal heating), several values of wall to wall spacing and different heating conditions. Gan[16] derived the general expressions for correlation of Nusselt number, Reynolds number and Rayleigh number and these expressions can be used for calculating the heat transfer rate and air flow rate in ventilation cavity for given height and width. The heat flux heat and distribution ratio can also be calculated. The experiments results were validated by other literature. Hughes and Ghani[18] studied the numerical simulation for feasibility of wind-vent. Computational fluid dynamics software (FLUENT) was used to simulate the model which was prepared in GAMBIT. It was investigated the effective utilization of fan pressure to achieve minimum natural ventilation during low external wind velocity $(1m/s)$. The bottom side fan location given maximum ventilation as compared to middle and top location in wind-vent.

No such studies like simulation and modelling of solar chimney for space heating are found in literature. And solar chimney proposed or used in all the literature can be used only for winter season to space heating, and insulation in the room have not considered. But in the present study, modified solar chimney (MS plate used as thermal mass) is integrated to an insulated experimental room which situated at CBRI Roorkee, India.

This study gives a novelty to use CFD for the study of solar chimney in space heating. The modified solar chimney system is the most prominent technique which can be used in building space heating for sustainable development. We can reduce energy demand used in space heating and ventilation up to some extent in residential and commercial buildings. The more research is needed by research tools to develop prototype and standardizing the solar chimney retrofit.

A model is a representation of a physical system that maybe used to predict the behavior of the system in desired respect. So the rigorous model analysis in CFD and results validation from experiment is required. To keep in mind the do and don't of passive system, numerical study in for feasibility of the modified solar chimney is presented in this paper. It will help us to understand, analyze and implement the solar chimney concept in the buildings and generate a solar chimney retrofit for existing buildings for passive space heating.

Table 1. Nomenclature

C	Constant	T	Temperature
C_p	Specific heat	t	Turbulence
f_p	Buoyancy force	U	Velocity
g	Gravitational constant	α	Absorptivity
h	Enthalpy	β	Coefficient of thermal expansion
k	Kinetic energy	ε	Energy dissipation
k_{eff}	Effective conductivity	μ	Dynamic viscosity
k_f	Fluid thermal conductivity	μ_t	Turbulent viscosity
k_t	Turbulent thermal conductivity	ρ	Density of air
p	Pressure	ρ_0	Reference density
p_{rt}	Turbulent Prandtl number	σ	Compressive stress
s_h	Source term with solar radiation		

2 CFD simulation strategy

We consider the steady turbulent flow model, so that Reynolds-Averaged Navier-Stokes equations (RANS) are used for modelling with $(k-\varepsilon)$ model. The Bousinesq approximation is used to account for air density variation in buoyancy flow. The dimensions of modelled solar chimney are shown in Tab. 2.

Table 2. Dimensions of modelled solar chimney

S.No.	Specifications	Dimensions (m)
1.	Absorber plate area	2.50
2.	Thickness of absorber plate (MS plate)	0.003
3.	Stack height	2.80
4.	Air gap between glazing and absorber plate	0.06
5.	Chimney height	3.10
6.	Dimension of inlet vent	0.30×0.30
7.	Dimension of outlet vent	0.30×0.30

The assumptions for this study of flow field and heat transfer distribution in collector are given as: steady-state, axisymmetric, collector model, ground model; All the calculations were determined with the Realizable $k-\varepsilon$ model and the basic equation summarized as below.

2.1 Basic equations

The realizable k-epsilon turbulent model with discrete ordinance radiation model for CFD simulation model has been adopted from [2, 21].The equation for transport phenomena developed by [13] have been used. The flow is assumed to be 2-D, steady and turbulent.

The Time Averaged Navier Stokes (TANS) equation for the mass and momentum transport are given by [21] as.

Continuity equation:

$$\frac{\partial u_i}{\partial x_i} = 0. \tag{1}$$

The momentum conservation equation:

$$\rho(u_j \frac{\partial u_i}{\partial x_j}) = \frac{p}{\partial x_j} + \frac{\partial}{\partial x_j}\left[(\mu + \mu_t)\frac{\partial u_i}{\partial x_j}\right] + f_b, \tag{2}$$

where buoyancy force is given by,

$$f_b = (\rho - \sigma_0)g. \tag{3}$$

The energy conservation is given by following transport equation,

$$\rho U_i \frac{h}{\partial x_i} = k_{eff}\frac{\partial}{\partial x_i}\left[\frac{T}{\partial x_i}\right] + S_h, \tag{4}$$

where effective conductivity is given by,

$$k_{eff} = k_f + k_t, \tag{5}$$

where, k_f is the fluid thermal conductivity and is turbulent thermal conductivity, the k_t is given by,

$$k_t = \frac{C_p \mu_t}{p_{rt}}. \tag{6}$$

And enthalpy (h) is given by,

$$h = \int_{T_n}^{T} C_p dT. \tag{7}$$

The calculation of energy equation source term is important because it incorporate the effect of radiation. In solid material the above equation is reduced to,

$$k_s \frac{\partial^2 T}{\partial x_i^2} + S_h = 0. \tag{8}$$

Turbulent Model: The flow inside the solar chimney is turbulent. The Realizable k-epsilon model implemented to solve the model, which is given by [23]. The transportation equation is in terms of turbulent kinetic energy (k) is given as:

$$\rho U_j \frac{\partial k}{\partial x_j} = \tau_{ij}\frac{\partial u_i}{\partial x_j} - \rho\varepsilon + \frac{\partial}{\partial x_j}\left[(\mu + \frac{\mu_t}{\sigma_k})\frac{\partial k}{\partial x_j}\right]. \tag{9}$$

The transportation equation is given in terms of heat dissipation rate as:

$$\rho U_j \frac{\partial \varepsilon}{\partial x_j} = C_{\varepsilon 1}\frac{\varepsilon}{k}P_k - \rho C_{\varepsilon 2}\frac{\varepsilon^2}{k} + \frac{\partial}{\partial x_j}\left[(\mu + \frac{\mu_t}{\sigma_\varepsilon})\frac{\partial \varepsilon}{\partial x_j}\right], \tag{10}$$

where, $\mu_t = \rho C_\mu \frac{k^2}{\varepsilon}$, $P_k = \tau_{ij}\frac{\partial u_i}{\partial x_j}$, $\sigma_k = 1$, $\sigma_\varepsilon = 1.3$, $C_\mu = 0.09$, $C_{\varepsilon 1} = 1.14$, $C_{\varepsilon 2} = 1.96$.

Radiation Model: The Discrete Ordinates (DO) model is used to simulate the MSC model. This model allows the solution of radiation at semi-transparent walls. DO radiation model solves the Radiative Transfer Equation (RTE) for a finite number of discrete solid angles, each associated with a vector direction $(\vec{s})$ fixed in the global Cartesian (x, y, z). It transforms RTE equation into transport equation for radiation intensity in the spatial coordinated (x, y, z). The RTE for solar irradiation intensity $[I_\lambda(\vec{r}, \vec{s})]$ turns to

$$\nabla(I_\lambda(\vec{r}, \vec{s})\vec{s}) + (\alpha_\lambda + \sigma_\lambda)I_\lambda(\vec{r}, \vec{s}) = \alpha_\lambda n^2 I_{b\lambda}(\vec{r}) + \frac{\sigma_s}{4\pi}\int_0^{4\pi} I_\lambda(\vec{r}, \vec{s'})\phi(\vec{s}, \vec{s'})d\Omega, \tag{11}$$

where, the spectral absorption coefficient (α_λ) can computed from the absorptivity (α) as per the media thickness (d).

$$\alpha_\lambda = \frac{1}{d}\ln\left(\frac{1}{1-\alpha}\right). \tag{12}$$

In this equation the phase function (ϕ- considered as isotropic), refractive index, scattering coefficient are assumed to be independent on wavelength. The angular apace (4π) at any spatial location is discretized into number solid angle (multiplication of polar and azimuthal angles) work as control of angles. The refractive index is taken as a constant in the calculation of black body emission as well as in the boundary conditions imposed by semi-transparent glass wall. Solving the fine angular discretization in DO model is CPU intensive, hence author have used a highly configured processor. The RTE is integrated over each length and total intensity in each direction can be computed by using [20],

$$I_\lambda(\vec{r}, \vec{s}) = \sum_k I_{\lambda k}(\vec{r}, \vec{s})\Delta\lambda_k. \tag{13}$$

This RTE equation coupled with a volumetric source term given by [23] as:

$$S_h = -\frac{\partial q_{ri}}{\partial x_i} = \alpha_\lambda\left[4\pi I_{b\lambda}(\vec{r}) - \int_0^{4\pi} I(\vec{r}, \vec{s})d\Omega\right]. \tag{14}$$

2.2 Computational effort

A Work station (Dell precision T7400 of 800MHz multi core Intel Xeon processors, 64GB RAM, 1TB HDD) needs less amount of computing time for one steady-state solution.

2.3 Boundary conditions

A static pressure boundary condition is used at chimney exit $(\Delta p_{out}(x) = 0)$. It means pressure at inlet and outlet of solar chimney is equal to atmospheric pressure. And the simulated inlet temperature of solar chimney is equal to the room temperature at same time which observed in the experiment.

2.4 Important input parameters

A 2-D steady, Realizable k-epsilon turbulent model with standard wall function is used for the study. Some of the important properties of materials and modelling parameters are required for the CFD simulation which is shown in Tab. 3 given as below. The molecular weight and viscosity of air is presented in Tab. 4.

3 CFD simulation modelling and meshing

The CFD simulation is working on step by step method which described as: to develop geometry, grid generation, putting boundary conditions, and simulate it in CFD up to convergence of model. The Realizable turbulent model with standard wall functions implies the two dimensional model.

Table 3. Properties of materials

Material	$\rho, kg/m^3$	$C_p, j/kg°C$	k, $W/m°C$	Emissivity	Absorptivity	Transmitivity
Mild Steel	7800	500	52	0.95	0.95	0
Glass	2500	820	1	0.9	0.06	0.84
Air	1.225	1006.43	0.0242			

Table 4. Molecular weight and viscosity of air

S.No.	Description		Unit	Particular/values
1	Air	Viscosity	$Kg/m-s$	1.7894×10^{-5}
		Molecular weight	$Kg/kg.mol.$	28.966

3.1 Geometry

A two Dimensional geometry based on designed dimensions mentioned in Tab. 1 is developed in design modular of workbench 14.0. After that grid is generated through meshing software. The quality of the grid/mesh plays a direct role on the quality of the analysis, regardless of the flow solver used. The grid can be shaped to be body fitted through stretching and twisting of the block. In the approach of the grid or mesh generation, we have modelled it for two approaches. In the first approach, the viscosity-affected the inner region and it is turbulent region and we used a wall function to bridge the viscosity affected region. In second approach this model is modified to enable the viscosity affected region to be resolved with mesh all the way to the wall. Mesh quality is the key for convergence and accurate CFD solutions especially for viscous flows over complex geometry. The skewness is an important factor to select the number of spacing count. The skewness factor (ψ) is the ratio of number of highly skewed element and the total element generated in grid/mesh generation, it varying between 0 and 1 and suitability of grid generation is that for which value of ψ must be low because highly skewed mesh dropdown the accuracy but convergent time will be less. Here we have select that interval number 70 which is appropriate number because the value of ψ is less or equal to 0.20 at 60 the ψ is 0.22 and for 80 it is 0.22 again for 100 it is higher and inverted negative elements also generated. The wall model requires that the wall distance to the middle of the next fluid cell be sufficiently small $y^+ < 1$. The developed geometry with meshing is shown in Fig. 2.

3.2 Mesh adoption

Mesh adoption is used to refine the mesh based on geometrical and numerical solution. Cells are in mesh, thus enabling the features of the flow field to be better resolved. When adoption is used properly than the resulting mesh is optimal for flow a solution which is necessary to refine the solution. In FLUENT click on a dialog box of adapt and after that click on boundary. This may perform by three different ways as number of cell (the distance of a cell from the boundary is measured in number of cells), normal distance and target boundary volume (cell refinement is based on a target boundary volume and growth rate). The parameters controlling the aspects of adaption is set in the mesh adoption control dialog box, and right mark on refine and coarse option and select the both fluid stator and fluid rotor.

Mesh can be improved by smoothing and swapping control, adapt swapping is used with triangular and tetrahedral cells; and smoothing is adapted for series cases not for parallel cases. Mesh adopted for the smooth flow of fluid in a solar chimney is shown in Fig. 3(a, b, c), and Fig. 2 shows results before mesh adoption. It is noted that the upper left and right bottom corner in exit vent (shown by blue mesh in Fig. 3 (a)) can be cut and solar chimney can be modified for smooth flow. In similar of that at lower end front bottom corner can be beveled in Fig. 3 (c) and this modification can improve the flow pattern as well as performance of solar chimney.

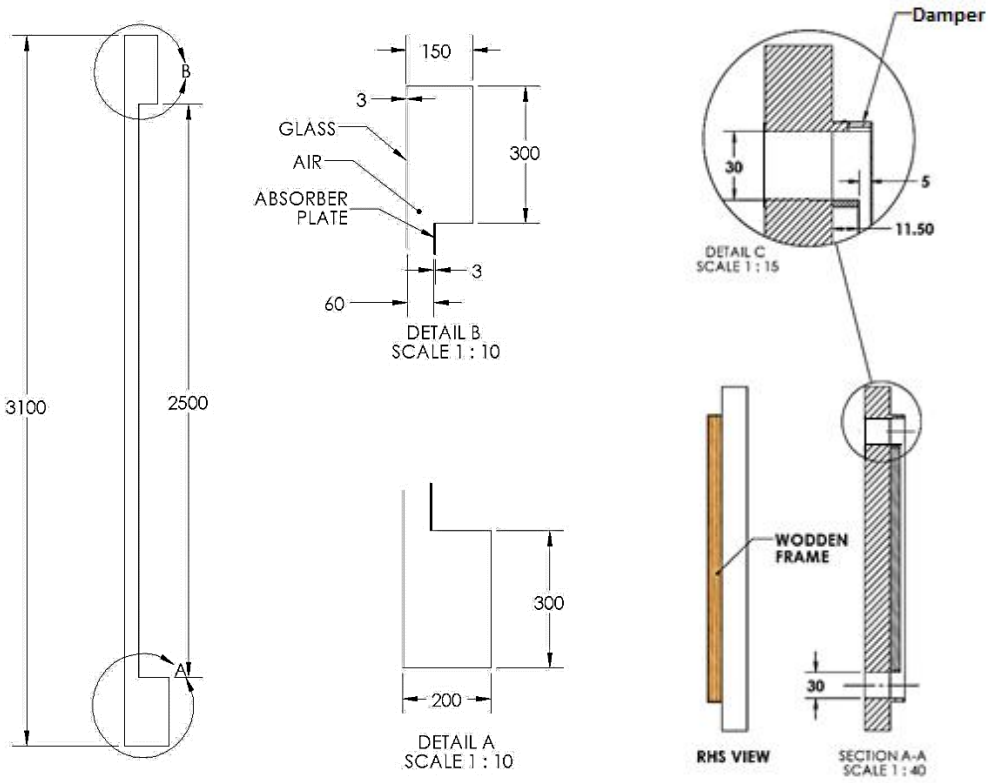

Fig. 1. Geometry of solar chimney for building space heating

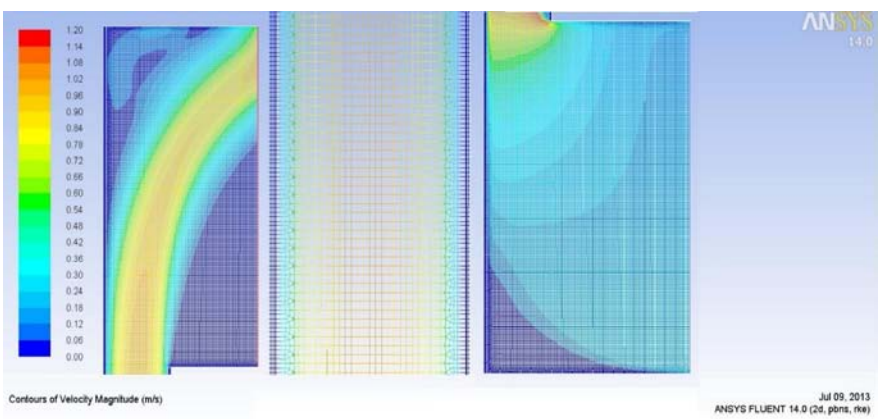

Fig. 2. Solar chimney air flow without mesh adaptation

4 Results and discussions

4.1 Model validation

The computational fluid dynamics model is operated under the experimental conditions and output results are shown in Tab. 5. The experimental and CFD simulated velocities for a typical day is presented in Fig. 4, and observed a small difference between exit velocities of experimental and CFD data , and it is found between 0.015 to 0.02 m/s. So a good agreement is found between experimental and CFD velocities. The plate temperature is not equal to the simulated results but there is little difference (0.48 to $1.62°C$) as shown in Fig. 5. And pattern would be similar for both velocity and temperature. It is found a good agreement between experimental and CFD simulated absorber plate temperatures. The BME and RSME are in acceptable limit (less than $\pm 5\%$).

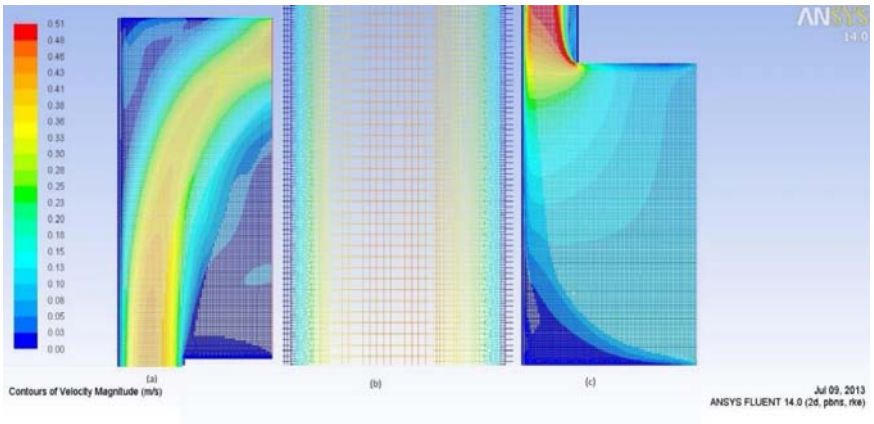

Fig. 3. Solar chimney air flow with mesh adaption

Table 5. Experimental and CFD simulated results

Date	Time hour	Global in W/m^2	Diffused in W/m^2	MS Plate Texp-R	Simulated Tscfd	Inlet u_i	Outlet u_0	Simulated $u_{i_{cfd}}$	Simulated $u_{0_{cfd}}$
10-12-2012	9	274.74	73.56	31.1	31.58	0.06	0.07	0.06	0.086
10-12-2012	10	434.23	89.46	37.7	39.94	0.13	0.16	0.13	0.181
10-12-2012	11	547.15	109.34	48.3	48.54	0.15	0.2	0.15	0.215
10-12-2012	12	576.25	101.39	51.1	51.81	0.16	0.21	0.16	0.229
10-12-2012	13	557.63	97.42	49.5	51.12	0.15	0.2	0.15	0.219
10-12-2012	14	428.41	95.43	40.5	41.19	0.15	0.18	0.15	0.211
10-12-2012	15	321.30	85.49	34.5	35.15	0.12	0.16	0.12	0.174
10-12-2012	16	136.20	57.65	24.4	25.48	0.06	0.07	0.06	0.086

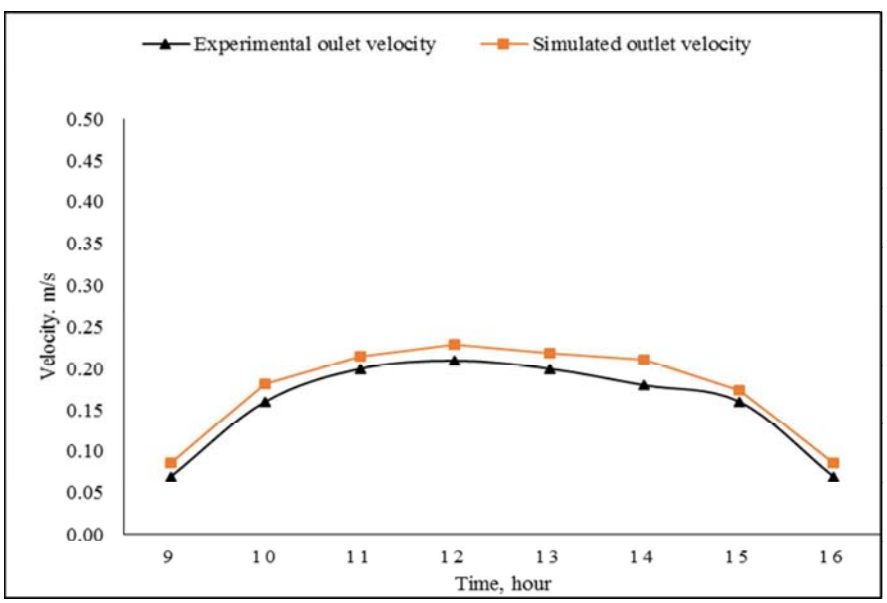

Fig. 4. Validation of MSC outlet velocity

4.2 Variation of air temperature between glazing and MS plate

Three horizontal rakes have been drawn at three positions in the CFD model to observe the temperature profile between the glass and plate. The Variation of temperature at rake $-1[(-3,-1250,0),(-63,-1250,0)]$, rake $-2[(-3,0,0),(-63,0,0)]$ and rake $-3[(-3,1250,0),(-63,1250,0)]$ is shown in Fig. 6, where series indicates the levels at lower middle and upper side of the solar chimney. At 12:00 hour of a particular day onrake-1, glass air temperature observed as minimum (Approx. $295K$) and highest at MS plate (approx. $304K$). The air temperature

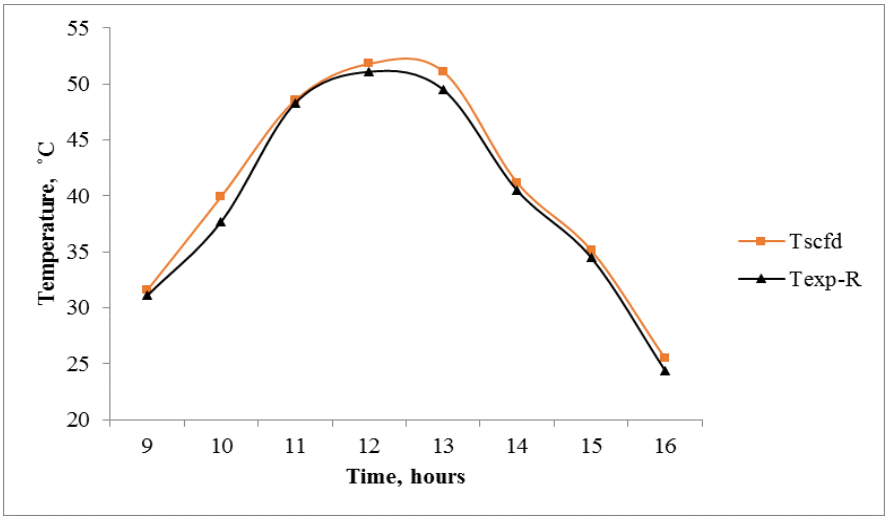

Fig. 5. Validation of MS plate (absorber) surface temperature

between rake (near plates) at position -0.01 and 0 (MS plate) decreases drastically, the air is bad conductor and perpendicular flow of heat is slower than the vertical. There is no higher difference between glass temperatures at all three levels. But the temperature difference of MS plate found significant (L-318K, M-326K and U-332K).

Again five vertical rakes have been drawn at five positions; their data are shown in Tab. 6. Fig.7 illustrate the variation of air temperature at distance 15, 30 and 45 mm from MS plate vertically. The air temperature of a rake near MS plate (15 mm) observed higher for throughout the length than the larger distance (30 and 45 mm) and it is increasing from bottom to upward direction. Temperature at 45 mm (Rake-18) is found higher than the temperature of Rake-17 (30 mm) it is due to that the Rake-18 lies near glass cover which having higher temperature.

Table 6. Rakes in vertical positions of solar chimney

Type	End points, mm
Rake$-$16	($-$18,1250,0), ($-$18,$-$1250,0)
Rake$-$17	($-$33,1250,0), ($-$33,$-$1250,0)
Rake$-$18	($-$48,1250,0), ($-$48,$-$1250,0)
Rake$-$19	($-$63,1250,0), ($-$63,$-$1250,0)
Rake$-$20	($-$3,1250,0), ($-$3,$-$1250,0)

4.3 Variation of MS plate and glass temperature

The absorber wall temperature is depends on its physical and thermal properties as well as on intensity of incident solar radiation. Fig. 8, expressed the variation of temperature over the MS plate, it increases from lower side to upward side. At inlet and exit position the experimental results seems low temperature than the CFD, it is because of at these positions room air is in directly contact with the inlet and exit point of MS plate. And for the other points, experimental results also represented the same pattern as CFD and there is no significant difference between both experimental and CFD results. For increasing the outlet temperature it recommended to increase the length of the absorber.

The variation of temperature of a glass cover (glazing) is shown in Fig. 9. It is appears that the losses from this single glazing is higher it is represented by the higher gap between the CFD and experimental results. Therefore, double glazing is recommended to decreasing the loss and increasing the performance of the solar chimney. The pattern of glass temperature variation is similar to the MS plate temperature variation.

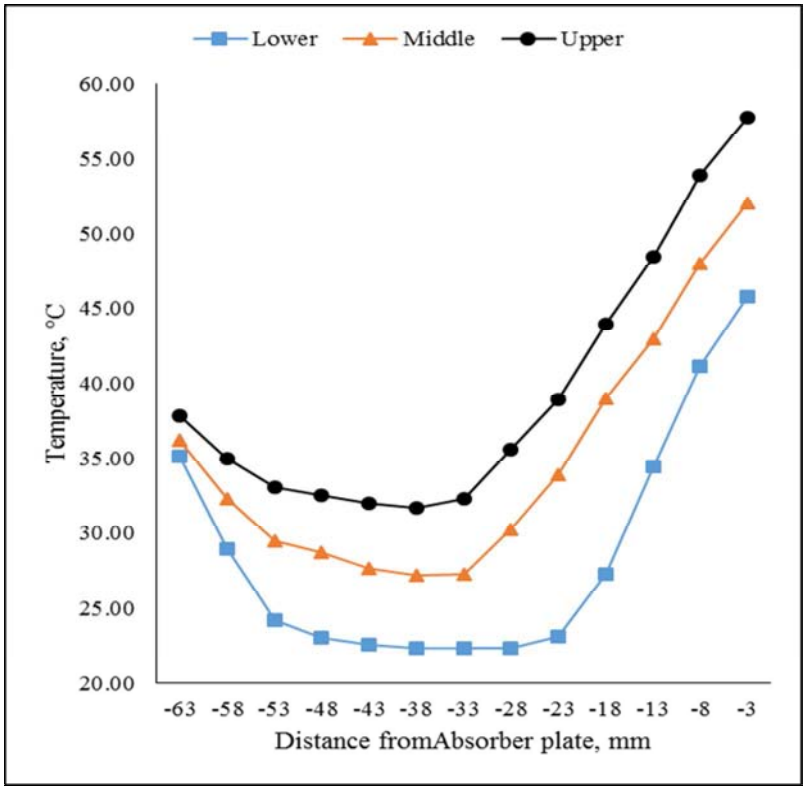

Fig. 6. Variation air temperature at three positions (lower, middle, and upper side)

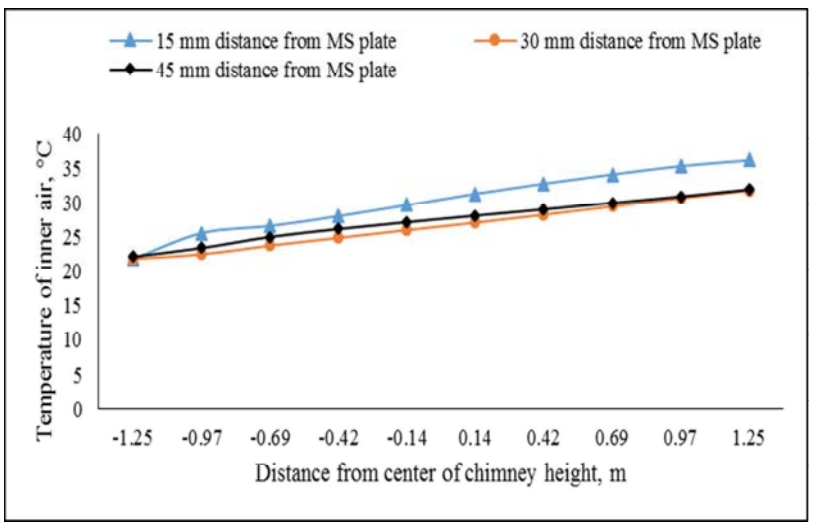

Fig. 7. Variation of air temperature in gap between MS plate and glass

4.4 Velocity and temperature profile

On the other hand, velocity contour in Fig. 10 indicates that the maximum velocity of air observed in middle of the gap. The flow in the upper portion of solar chimney clearly indicates that there is no use of blue portion at downward side of yellow or orange shades. We can remove that portion and solar chimney can be modified accordingly, so the reverse flow and losses can be reduced. A heat sink zone at bottom of entry section of solar chimney is developed as shown in temperature contour of Fig. 11 and it may be reduced in modified design of solar chimney. Both the Figures shows that the temperature and flow field profiles are not symmetric to the center line of the air channel of solar chimney as expected because of the difference between the glazing and MS plate temperatures.

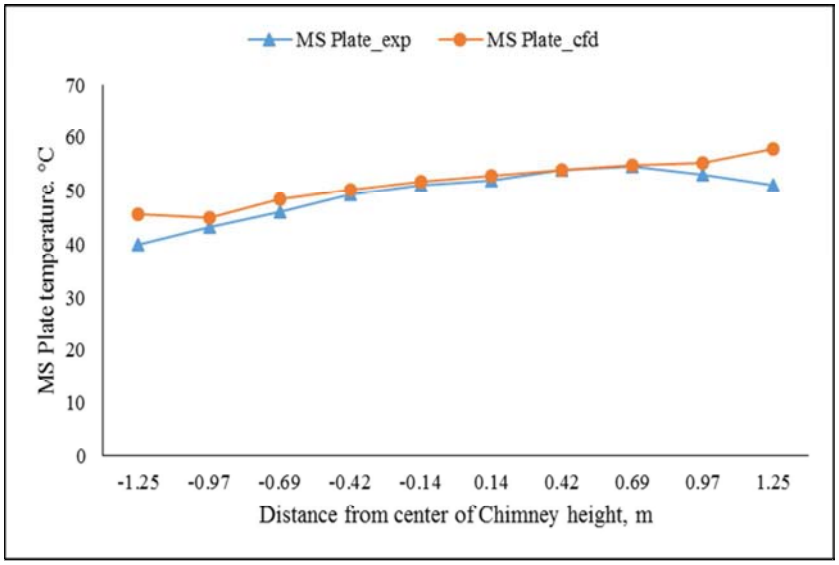

Fig. 8. Variation of MS plate temperature at particular time

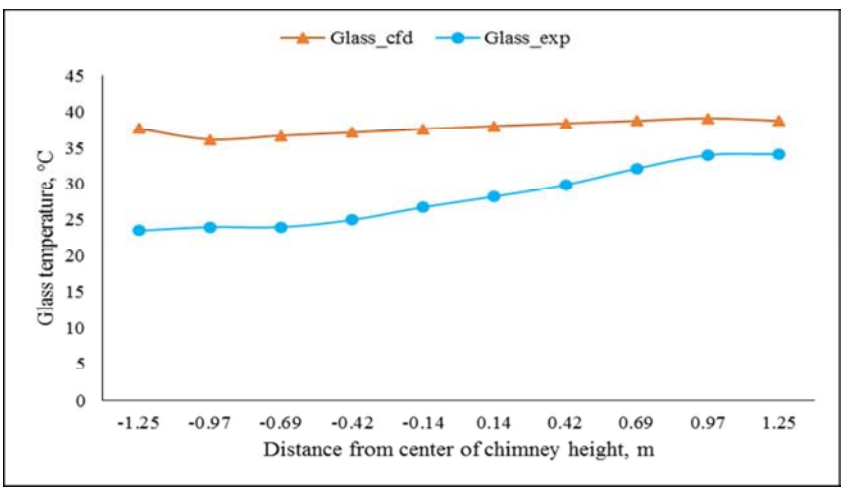

Fig. 9. Variation of glass temperature at particular time

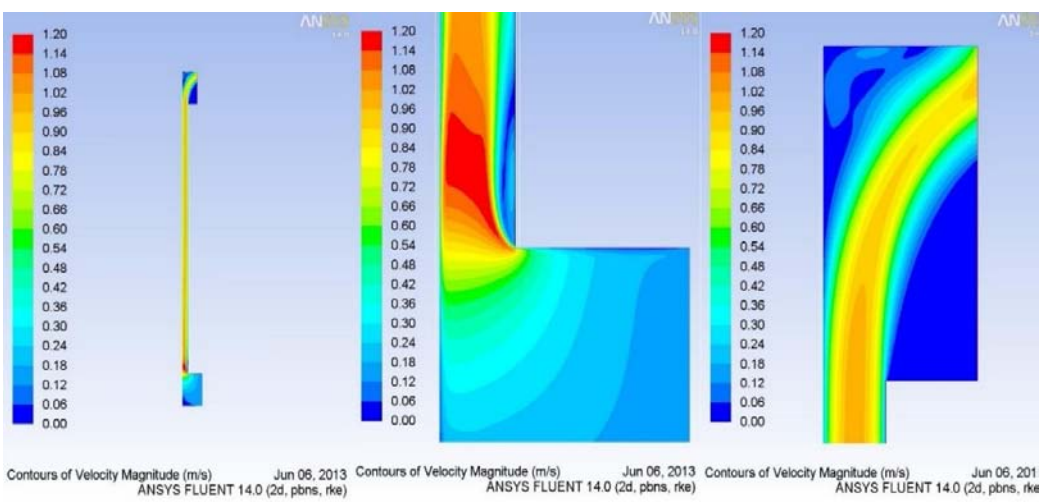

Fig. 10. Velocity contour

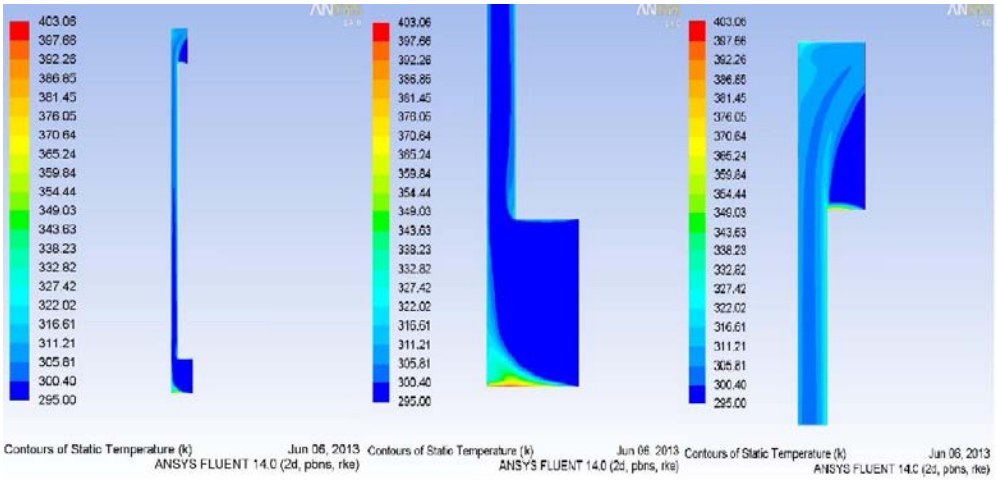

Fig. 11. Temperature contour

4.5 Variation of velocity with air gap

The outlet velocity from the CFD simulation is represented for three different air gaps as shown in Fig. 12. From the CFD simulation at three different air gaps as: $6cm$, $10cm$, and $14cm$, it is found that the air velocity for $14mm$ air gap is higher than the other two air gaps and difference is uniform throughout the day. It means the air gap is affected the outlet velocity of solar chimney if air gap is higher means increases the air velocity. So we recommended for larger air gap.

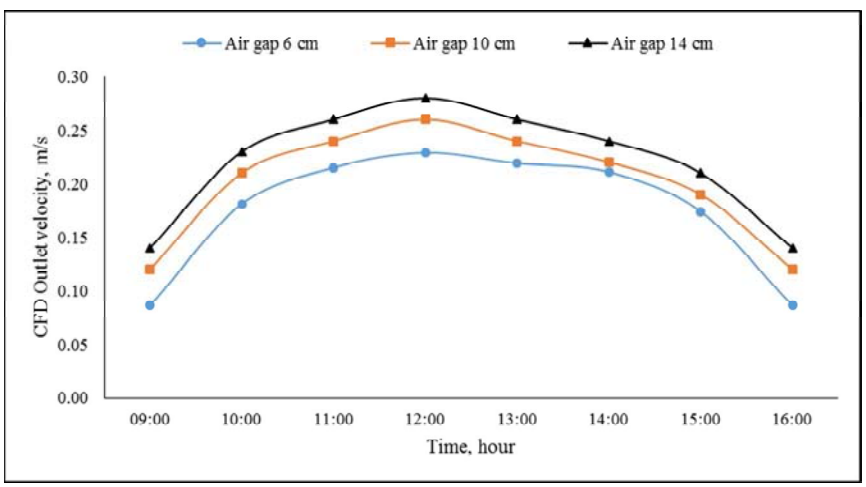

Fig. 12. Variation of outlet air velocity with air gap

4.6 Stack effect

The stack ventilation (buoyancy ventilation) can be induced by temperature difference. A proper temperature difference is needed for significant stack ventilation. As the warm air, which is less dense or lighter, rises in the solar chimney. This is shown in Figs. 13 and 14, where inlet side found higher pressure than outlet side. The pressure difference for a typical day is shown in Tab. 7. It is revealed that the higher net pressure difference found at 12 noon and it is found in face of solar radiation availability.

Table 7. Pressure variation for a particular day on winter 2012

S.No.	Time hour	Inlet Pascal	Outlet Pascal	Net Pascal
1	09:00	0.11000	−3.54000	0.05457
2	10:00	0.98600	−0.00030	0.49313
3	11:00	0.98460	−0.00032	0.49313
4	12:00	1.09900	−0.00035	0.54933
5	13:00	0.98450	−0.00040	0.49208
6	14:00	0.98466	−0.00026	0.49220
7	15:00	0.67400	−0.00025	0.33690
8	16:00	0.21150	−6.56824	0.10571

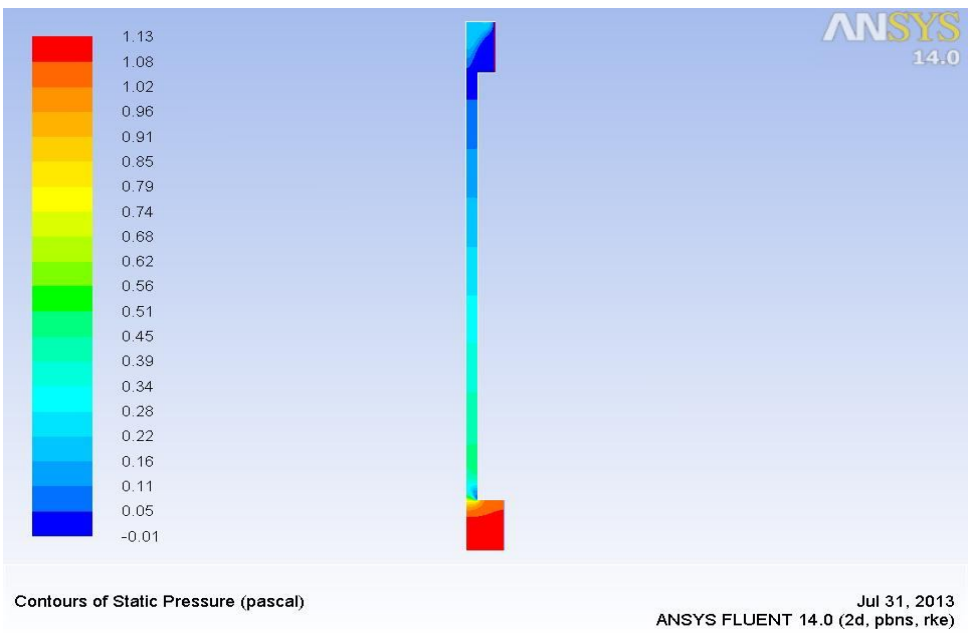

Fig. 13. Static pressure variation in modified solar chimney

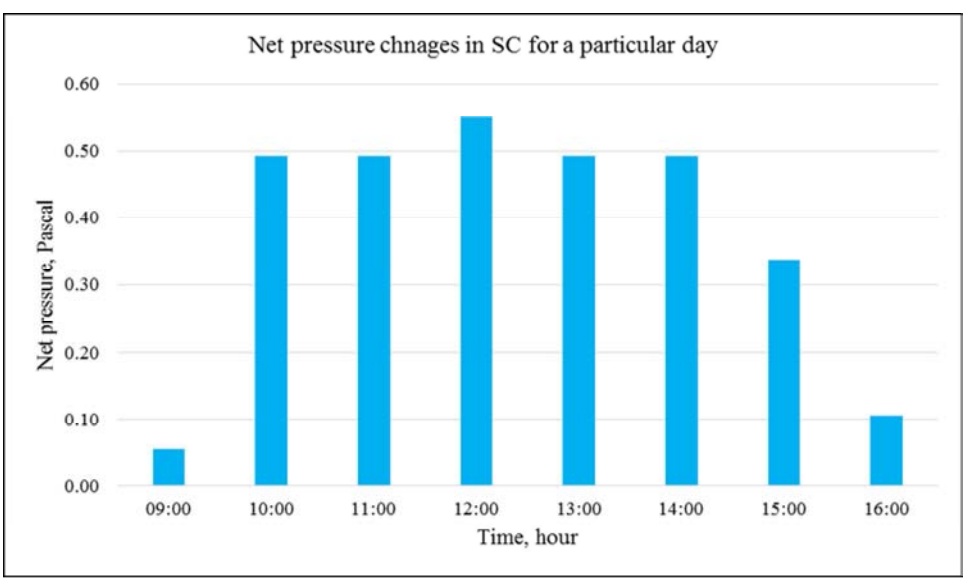

Fig. 14. Net pressure changes in modified solar chimney

5 Conclusions

CFD analysis of a modified solar chimney have been analyzed and validated using experimental data collected at CBRI Roorkee, India in the month of December 2012 and found a good agreement between experimental and simulated results. It is found that the air temperature evaluated lowest ($20-35^{\circ}C$) at the middle of solar chimney gap and highest near the absorber plate ($45-65^{\circ}C$). The experimental room temperature have been maintained between $10^{\circ}C$ to $20^{\circ}C$ (Comfort temperature) in peak winter season, where ambient temperature was observed as $3^{\circ}C-8^{\circ}C$. Its cost is low due to selection of low cost materials. Hence it is a feasible solution for space heating in winter.

This study is recommended the higher absorber length, double glazing and higher air gap required for higher temperature production. This study can be used for future research for different absorber plate (variable thermal mass) and glass materials for enhanced thermal performance.

The study shows that the CFD is a useful tool for investigating the possibilities of a proposed device prior to prototype and testing. It is helpful in development of solar chimney retrofit for existing buildings.

References

[1] Ansys workbench 14.0, ansys, inc. canonsburg, pennsylvania, U.S.A.

[2] http://www.cfd-online.com/wiki/standard_k-epsilon_model.

[3] A. Akbarzadeh, W. Charters, D. Lesslie. Thermo-circulation characteristics of a trombe wall passive cell. *Solar Energy*, 1982, (28): 461–468.

[4] H. Awbi, G. Gan. Simulation of solar-induced ventilation. *Renewable Energy Technology and the Environment*, 1992, (4): 16–30.

[5] E. Bachoroudis, M. Vrachopoulos, et al. Study of the natural convection phenomena inside a wall solar chimney with one wall adiabatic and one wall under a heat flux. *Applied Thermal Engineering*, 2007, **27**(13): 2266–2275.

[6] N. Bansal, J. Mathur, M. Bhandari. Solar chimney for enhanced stack ventilation. *Building and Environment*, 1993, (28): 373–377.

[7] G. Barozzi, M. Imbabi, et al. Physical and numerical modelling of a solar chimney-based ventilation system for buildings. *Building and Environment*, 1992, (27): 33–45.

[8] R. Bassiouny, N. Korah. Effect of solar chimney inclination angle on space flow pattern and ventilation rate. *Energy and Buildings*, 2009, **41**(2): 190–196.

[9] R. Bassiouny, N. Koura. An analytical and numerical study of solar chimney use for room natural ventilation. *Energy and Buildings*, 2008, **40**(5): 865–873.

[10] A. Bouchair. Solar chimney for promoting cooling ventilation in southern Algeria. *Building Service Engineering, Research and Technology*, 1994, (15): 81–93.

[11] A. Bouchair, D. Fitzgerald, J. Tinker. Moving air using stored solar energy. *Proceedings of the 13th National Passive Solar Conference Cambridge*, 1988, 8–33.

[12] Z. Chen, Y. Li. A numerical study of a solar chimney with uniform wall heat flux. *Proceedings of the Fourth International Conference on Indoor Air Quality, Ventilation and Energy Conservation in Buildings, Hunan China*, 2001, 1447–54.

[13] J. Ferziger, M. Peric. Computational methods for fluid dynamics. *Springer Berlin*, 2002.

[14] D. Fidaros, C. Baxevanou. Numerical study of the natural ventilation in a dwelling with solar chimney. *Third international conference EPALENC, Rhodes island Greece*, 2010, 1–12.

[15] G. Gan. A parametric study of trombe walls for passive cooling of buildings. *Energy and buildings*, 1998, (27): 37–43.

[16] G. Gan. General expressions for the calculation of air flow and heat transfer rates in tall ventilation cavities. *Building and Environment*, 2011, **46**(10): 2069–2080.

[17] G. Gan, S. Riffat. A numerical study of solar chimney for natural ventilation of buildings with heat recovery. *Applied Thermal Engineering*, 1998, (18): 1171–1187.

[18] B. Hughes, S. Ghani. A numerical investigation into the feasibility of a passive-assisted natural ventilation stack device. *International Journal of Sustainable Energy*, 2011, **30**(4): 193–211.

[19] J. Khedari. Ventilation impact of a solar chimney on indoor temperature fluctuation and air change in a school building. *Energy and Buildings*, 2000, (32): 89–93.

[20] S. Kim, K. Huh. A new angular discretization scheme of the finite volume method for 3-d radiative heat transfer in absorbing, emitting and an isotropically scattering media. *International Journal of Heat and Mass Transfer*, 2000, **43**(7): 1233–1242.

[21] S. Lal. Experimental, cfd simulation and parametric studies on modified solar chimney for building ventilation. *Applied Solar Energy*, 2014, **50**: 37–43.

[22] S. Lal, S. Kaushik, P. Bhargava. A study on stack ventilation system and integrated approaches. *Conference on Emerging Trends of Energy Conservation in Buildings*, 2012, (1-3): 255–263.

[23] B. Launder, D. Spalding. The numerical computation of turbulent flows. *Computer Methods in Applied Mechanics and Engineering*, 19742, **3**(2): 69–289.

[24] W. Lipping, L. Angui. A numerical study of vertical solar chimney for enhancing stack ventilation in buildings. *The 21th Conference on Passive and Low Energy Architecture. Eindhoven, Netherlands*, 2004, 1–5.

[25] H. Nouanegue, L. Alandji, E. Bilgen. Numerical study of solar-wind tower systems for ventilation of dwellings. *Renewable energy*, 2008, **33**: 434–443.

[26] K. Ong. A mathematical model of a solar chimney. *Renewable Energy*, 2003, (28): 1047–1060.

[27] K. Ong, C. Chow. Performance of a solar chimney. *Solar Energy*, 2003, (74): 1–17.

[28] L. Zalewski, S. Lassue, et al. Study of solar walls- validating a numerical simulation model. *International Review on Building and Environment*.

[29] B. Zamora, A. Kaiser. Optimum wall-to-wall spacing in solar chimney shaped channels in natural convection by numerical investigation. *Applied Thermal Engineering*, 2009, **29**(4): 762–769.